

A Computer Heart Model Incorporating Anisotropic Propagation

I. Model Construction and Simulation of Normal Activation

Michel Lorange, PhD, and Ramesh M. Gulrajani, PhD

Abstract: Present-day computer models of the entire heart, capable of simulating the activation isochrones and subsequently the body surface potentials, focus on considerations of myocardial anisotropy. Myocardial anisotropy enters into play at two levels, first by affecting the spatial pattern of activation owing to faster propagation along cardiac fibers and second by altering the equivalent dipole sources used to calculate the surface potentials. The construction of a new and detailed model of the human heart is described, based on 132 transverse sections obtained following a computed tomography scan of a frozen human heart whose chambers were inflated with pressurized air. The entire heart anatomy was reconstructed as a three-dimensional array of approximately 250,000 points spaced 1 mm apart. Conduction in the thin-walled atria was assumed isotropic from the sinus node region to the atrioventricular node, where it was subject to a 50 ms delay. A two-tier representation of the specialized conduction system was used, with the initial segments of the left and right bundles represented by a system of cables that feeds to the second tier, which is a sheet of conduction tissue representing the distal Purkinje system. Approximately 1,120 "Purkinje-myocardium" junctions present at the terminations of the cables and sprinkled uniformly over the sheet, transmit the excitation to the ventricles. A stylized representation of myocardial fiber rotation was incorporated into the ventricles and the local fiber direction at each model point used to compute the velocity of propagation to its nearest neighbors. Accordingly, the activation times of the entire ventricular myocardium could be determined using the 1,120 or so Purkinje-myocardium junctions as start points. While myocardial anisotropy was considered in the ventricular propagation process, it was ignored in the computation of the equivalent dipole sources. Nevertheless, the computed electrocardiogram, vectorcardiogram, and body surface potential maps obtained with the new heart model properly positioned inside an inhomogeneous torso model were all within normal limits. **Key words:** heart model, anisotropic propagation, computer simulation, isochrones, electrocardiographic potentials.

From the Research Center, Hôpital du Sacré-Coeur and Institute of Biomedical Engineering, Ecole Polytechnique et Université de Montréal, Montreal, Quebec, Canada.

Supported by Program Grant PG-11190 from the Medical Research Council of Canada and by a Graduate Research Fellowship to M. Lorange from la Fondation des Diplômés de Polytechnique.

Reprint requests: Ramesh M. Gulrajani, PhD, Research Center, Hôpital du Sacré-Coeur, 5400 West Gouin Boulevard, Montreal, Quebec, Canada H4J 1C5.

Present-day computer models of the entire heart,^{1,2} capable of simulating the activation isochrones and subsequently the surface electrocardiogram (ECG), vectorcardiogram (VCG), and body surface potential map (BSPM), focus on considerations of myocardial anisotropy. The spiral-layered structure of the ventricular myocardium gives rise to a spatially varying electrical anisotropy that enters into play at two levels, first by affecting the spatial pattern of activation owing to faster propagation along cardiac fibers and second by altering the equivalent dipole sources used to calculate the surface potentials. Here, we describe the construction of a new and detailed model of the human heart, based on computed tomography (CT) scans taken at autopsy, that includes a stylized representation of fiber direction in the ventricles according to the data of Streeter et al.^{3,4} The heart model, which comprises atria as well as ventricles, also includes a stylized representation of the His-Purkinje conduction system affixed to its endocardial surface. This study describes the activation isochrones generated by the model for the case of normal excitation, together with the normal ECG, VCG, and BSPM obtained when the new heart model was implanted within an inhomogeneous torso model. The anisotropic nature of the ventricles was taken into account in the simulation of the activation isochrones, but not in the calculation of the equivalent dipole sources. The companion article⁵ describes the activation isochrones, ECGs, VCGs, and BSPMs obtained when propagation was either completely blocked or significantly delayed at different sites along the conduction system and compares the simulations of the conduction blocks or delays to textbook cases of the same conduction abnormalities.

Materials and Methods

Reconstruction of Heart Anatomy

The traditional method used for computer reconstruction of heart anatomy is to inject warm liquid gelatin under diastolic pressures into the heart chambers, freeze the injected heart, and subsequently slice it at 1-mm intervals.⁶ The slices are then photographed, and the photographs digitized for entry into the computer. Our original intention was to use this procedure, except rather than slice the heart, we simply intended to obtain slice geometry via CT scans. When this modified procedure was tried on a canine

heart, we found the difference in density between the frozen gelatin and cardiac tissue too small to permit accurate separation of the gelatin-heart boundary from the CT scan slices. Much better separation was obtained with an air-heart interface, which led us to adopting the procedure described below.

A human heart, with its blood vessels cut away at some distance from the myocardium, was obtained at autopsy. The four chambers were dried by suction, and all blood vessels ligated, except the aorta and pulmonary artery, which were cannulated for the purpose of inflating the left and right sides with air at end-diastolic pressures of 8 and 4 mmHg, respectively. The inflated heart was then submerged in liquid nitrogen, freezing it almost instantly. The frozen heart was kept at -70°C awaiting a CT scan.

The CT scan was performed with the heart aligned so as to have its atrioventricular ring parallel to the plane of the scan. This was confirmed by taking a preliminary tomographic slice at the level of the atrioventricular ring. The CT scanner (Picker, Model 1200SX) produced 132 slices of 1-mm thickness taken at 1-mm intervals. Each slice resulted in a 512 by 512 pixel image, with a 12-bit digitized gray scale. The images were stored on magnetic tape for off-line processing on a 36 MHz Silicon Graphics Personal Iris workstation (Model 4D/35G) using special routines written at our institution for the three-dimensional reconstruction of biologic structures from serial sections.^{7,8}

Image segmentation techniques were used to first separate the high-contrast air-heart interface using an appropriate gray scale threshold. Next, the narrow gray scale range that spanned the low-contrast fat-myocardium interface was expanded to 256 levels, and a second segmentation threshold to distinguish fat from myocardium was determined. It is important to separate fat from myocardium since the former tissue, found largely around the atrioventricular ring and outer surface of the heart, is nonconducting and serves to electrically isolate the atria and ventricles. Each segmented slice was stored in computer memory as a two-dimensional matrix of points spaced 0.5 mm apart. The 132 slices were aligned and stacked by computer to eventually regenerate the cardiac anatomy as a three-dimensional matrix of approximately 250,000 points spaced 1 mm apart.^{9,10}

A major difficulty arose due to the onset of rigor mortis. We could only receive the human heart approximately 4–5 hours after death on account of autopsy consent procedures, and accordingly rigor mortis had set in. As a result, the air pressures used, while more than adequate to inflate the thin-walled atria, could not fully open the thick-walled ventri-

cles. Moreover, it was not possible to increase these pressures for fear of tearing the atria. Therefore, in the interest of obtaining correct simulations we had to "open" the ventricular cavities of the heart model by removing part of the endocardial layer all around the left ventricle and by deepening the narrow apical region of the right ventricle. This difficulty is not particular to the air-inflation technique used and will also occur with gelatin-injection techniques if similar delays in obtaining a human heart are experienced. One disadvantage of having to open the ventricular cavities manually is that it almost eliminated the papillary muscle anatomical structures at the endocardium.

Representation of Cardiac Conduction

Normal excitation of the heart model was initiated in the right atrium at its junction with the superior vena cava, in accordance with the experimental observations in dogs of Boineau et al.¹¹ indicating that this area, which encompasses the sinus node region, is the site of earliest activation. Three initiation zones around the superior vena cava were used, each comprising from four to five model points. This multiple origin of atrial depolarization is in accordance with the observations of Boineau et al.¹¹ It also permitted some flexibility in controlling atrial excitation patterns. Normally all three initiation zones were excited within 10 ms of each other. Excitation of the thin-walled and essentially two-dimensional atria was achieved by assuming isotropic spread, at a velocity of 79 cm/s, from these initiation zones. This velocity was chosen so as to excite the atria in 120 ms in keeping with the average P wave duration measured in man.¹² Boineau et al.¹³ reported atrial propagation velocities between 30 and 110 cm/s depending on the direction of propagation, and our velocity represents an approximate average consistent with our assumption of isotropic propagation. With this average velocity, no specification of specialized fast conducting pathways was necessary, although it must be remembered that the convoluted atrial surface that results due to its interruption by the many blood vessels in effect defines separate conduction pathways between the sinus and atrioventricular nodal regions. The atrioventricular node was represented as a collection of 17 model points in the interatrial septum, through which propagation speed was reduced to 2.4 cm/s, resulting in a 50-ms delay. A set of 25 model points with a propagation speed

of 2.5 m/s and an additional 5-ms delay represented the common His bundle.

A two-tier model was used for the rest of the specialized conduction system. The initial segments of the left and right bundles were represented by a system of cables of progressively diminishing conduction velocities that fed a sheet of conduction tissue representing the distal Purkinje network. Experimental observations in dogs of regular endocardial activation isochrones, with very little discontinuities,^{14,15} suggest that the distal network can be functionally represented as a sheet. The conduction velocities used diminished from 2 to 1 m/s for the cable portion of the conduction system, but were kept fixed at 1 m/s for the sheet portion. While the cable portion of the conduction system was overlayed on the endocardial surface of the heart model, the sheet portion was embedded into and formed part of the innermost endocardial layer of model points. The ventricles were excited via approximately 1,120 Purkinje-myocardium junctions present at the terminations of the cables, as well as uniformly sprinkled on the sheet representation of the Purkinje network. A fixed delay of 3 ms was introduced at each junction, in keeping with reported observations in dogs of junctional delays between 2 and 4 ms.^{16,17} The earliest regions of the ventricles to be excited were via the junctions at the cable terminations. In the left ventricle three separate cable networks excited the midseptum, the high anterior paraseptal and low anterior papillary muscle regions, and finally the posterior papillary muscle region, respectively. In the right ventricle a single cable network excited the lower right septum, apex, and right ventricular free wall in the region of the anterior papillary muscle. These sites are all close to those described by Durrer et al.¹⁸ as being the earliest to be activated. The cable portion of the conduction system, in effect, controlled the relative excitation times of these different regions. Thus, in the left ventricle the midseptal region was excited first, 160 ms after the start of sinus node activity, and the high anterior paraseptal and low anterior and posterior papillary muscle regions 3, 14, and 19 ms later, respectively. The greater delay in the excitation of the anterior and posterior papillary muscle regions in relation to the excitation times measured by Durrer et al.¹⁸ may be attributed to the greater penetration of the cable system into the ventricular subendocardium due to the elimination of the papillary muscle structure. Excitation of the right septum and anterior papillary muscle in the right ventricle followed left ventricular septal excitation by 7 and 8 ms, respectively. The advantage of utilizing a cable structure was the ease it afforded in simulating the conduction

blocks by simply blocking conduction at a cable site.⁵ The embedding of the distal sheet representation in the endocardial layer, on the other hand, permitted the simulation of conduction in the distal Purkinje network and in the ventricular myocardium as a single combined simulation. This has the advantage that during the simulation of the conduction blocks, reentrant activation of Purkinje tissue from ventricular muscle could be very conveniently incorporated.

Only in the thick-walled ventricles was the propagation of cardiac excitation assumed to be anisotropic. It is well known that the cardiac fibers in the ventricular myocardium lie roughly parallel to the endocardial and epicardial surfaces. If the fiber direction is examined across the ventricular walls, the fiber angle α , measured in the plane of the wall relative to the plane of the atrioventricular ring, rotates, on average, 120° from endocardium to epicardium.^{3,4} To approximate this structure, a stylized representation of the ventricles was used. The left and right ventricles were each characterized by a family of nested ellipsoids of revolution extending from endocardium to epicardium, with α varying 120° from the endocardial ellipsoid to the epicardial ellipsoid. In this manner, by determining which ellipsoid passes through a particular model point, the local fiber direction at the point can be inferred. More precise determination of fiber orientation was deemed unnecessary, given that our major interest was in simulating body surface potentials at some distance from the heart and that other limiting approximations were to be used in determining these potentials.

For any ventricular model point, the velocity $v(\hat{a})$ for propagation along a direction characterized by the unit vector \hat{a} is given by¹⁹

$$(1) \quad v(\hat{a}) = K \left[\frac{(\hat{a}^* G_i \hat{a})(\hat{a}^* G_o \hat{a})}{\hat{a}^*(G_i + G_o)\hat{a}} \right]^{1/2}$$

where K is a proportionality constant, the asterisk denotes the transpose, and G_i and G_o are the diagonal intracellular and interstitial conductivity tensors, respectively. Equation 1 assumes a cartesian coordinate system with one axis (z) aligned along the local fiber direction, and accordingly, G_i and G_o are given by

$$(1a) \quad G_i = \begin{bmatrix} g_{it} & 0 & 0 \\ 0 & g_{it} & 0 \\ 0 & 0 & g_{il} \end{bmatrix}, \quad G_o = \begin{bmatrix} g_{ot} & 0 & 0 \\ 0 & g_{ot} & 0 \\ 0 & 0 & g_{ol} \end{bmatrix}.$$

The conductivities g_{it} and g_{il} are, respectively, the intracellular conductivities transverse and parallel to the cardiac fibers, with g_{ot} and g_{ol} similar conductivities for the interstitial space. These conductivities are

effective conductivities obtained by assuming the myocardium to be an anisotropic bidomain. Their numerical values are $g_{it} = 0.0263 \text{ S/m}$, $g_{il} = 0.278 \text{ S/m}$, $g_{ot} = 0.133 \text{ S/m}$, and $g_{ol} = 0.222 \text{ S/m}$. These values are the same as those given by Plonsey and Barr²⁰ and are based on the experimental measurements of Roberts et al.²¹ on canine myocardium. Equation 1 was used to define the velocity of propagation from any model point to its nearest neighbors. The local direction of anisotropy was taken into account by always using a coordinate system with the z axis aligned along the fiber direction. The constant K was adjusted so that the longitudinal and transverse velocities were 63 and 22 cm/s, respectively. These values are comparable to the 58 and 25 cm/s reported by Roberts et al.^{21,22} in canine myocardium. Knowing the velocity of propagation from one model point to the next, the activation times of the entire ventricular myocardium could be determined using the 1,120 or so Purkinje-myocardium junctions as start points. If a particular model point was excited at different times from two or more of its neighbors, only the earliest time was conserved and used as the correct time of activation.

Computation of Surface Potentials

Computation of surface potentials follows the usual approach of first defining a transmembrane action potential for each model point whose onset coincides with the activation time of the point in question. Next, from the action potential waveforms and onset times the spatial distribution of the transmembrane potential can be obtained. The spatial gradient of this distribution is converted into equivalent dipole sources, and these equivalent sources are then used to generate the surface potentials once the heart model is placed within a numerical torso model.

Digitized representations of typical action potential waveforms for the sinus node, atria, atrioventricular node, Purkinje cell, and ventricles given by Katz²³ were used for the corresponding model points. No computations of the spatial transmembrane distribution were performed, however, for either the cable or the sheet portions of the specialized conduction system, and hence the model does not generate any His-Purkinje surface ECG deflection. With regard to ventricular action potentials, it is well known that their durations shorten from endocardium to epicardium, and also from apex to base,^{24,25} and accordingly this shortening was introduced into the model as reductions in the duration of the plateau of the ventricular action potential. The durations of the

longest and shortest action potentials were 280 and 220 ms, respectively, and were chosen so that T wave waveforms and amplitudes appeared reasonable.

As mentioned earlier, myocardial anisotropy also affects the computation of the "far-field" body surface potentials by affecting the equivalent dipole sources. Here, however, the equivalent dipole sources were obtained assuming an isotropic bidomain model for the myocardium. In effect, the equivalent dipole density \vec{m} , assumed to exist in the interstitial space, is given by²

$$(2) \quad \vec{m} = -\frac{g_i g_o}{g_i + g_o} \nabla V_m,$$

where g_i and g_o are the isotropic intracellular and interstitial conductivities and V_m is the transmembrane potential distribution. This was largely because no exact and computationally tractable formulation similar to equation 2 exists for a bidomain heart model with unequal anisotropy ratios in the intracellular and interstitial media and varying fiber direction placed within a realistic torso model. The values selected for g_i and g_o were 0.1 and 0.2 S/m, respectively. The value for g_i lies between the estimates of g_{it} and g_{il} as determined by Roberts et al.,²¹ and the value for g_o is between those for g_{ot} and g_{ol} . The value for g_o was deliberately chosen to be equal to the conductivity value used for the torso so as to eliminate a conductivity interface between interstitial space and torso, thereby simplifying surface potential computations. Note that equation 2 is less suitable for "near-field" epicardial potential calculations on account of the extreme proximity of the epicardium to the elemental dipoles being inconsistent with the spatial averaging implied in assuming an isotropic bidomain model for the myocardium.

Surface potential computations were achieved by first subdividing the heart model into 88 regions (25 atrial and 63 ventricular) and combining the individual dipole densities within each region. The resultant dipoles for each region were assumed to act at the region centroids and used to compute the ECG, VCG, and BSPM once the model heart was placed within the torso model. An inhomogeneous torso model of base conductivity 0.2 S/m was used, with separate regions representing the intraventricular blood masses (conductivity 0.6 S/m), lungs (0.05 S/m), and a skeletal muscle layer. The anisotropy of the muscle layer was realized using the torso extension approach suggested by McFee and Rush²⁶ and described by Gulrajani and Mailloux,²⁷ wherein a 1-cm thick anisotropic skeletal muscle layer is tripled in thickness but replaced with an isotropic conductivity (0.125 S/m). Indeed, the torso model and surface potential computation techniques used by us are identical to

those described by Gulrajani and Mailloux, the only exception being that the geometry of the intraventricular blood masses was altered to conform to the internal cavities of the new heart model.

Correct excitation of the heart model was an iterative trial and error process in which parameters of the conduction system, such as geometry, conduction velocity, and its junctions with the ventricular myocardium, were altered so as to first result in activation isochrones that were qualitatively acceptable. Next the body surface potentials were computed, and further iterative adjustment of conduction system parameters and heart orientation was performed so as to result in a "normal" ECG, VCG, and BSPM. The generation of normal surface potentials, particularly a normal VCG, represents a much more stringent test of correct activation than simply activation isochrones that are qualitatively normal, since the relative time difference between the excitation times of the two ventricles comes into play in the surface potential computations. The correctness of this relative time difference is very difficult to gauge from just a qualitative look at the activation isochrones.

Results

All computations were performed on a 36 MHz Silicon Graphics Personal Iris workstation (Model 4D/35G, with 16 MB memory, 380 MB disk storage, 24 color bitplanes, plus a 24-bit Z buffer). Several of the figures were prepared using TECPLOT, a commercial plotting package (Amtec Engineering, Bellevue, WA).

Anatomic Representation

Plate 1 is a photograph of the inflated human heart, and Plate 2 is a three-dimensional view of the reconstructed model heart from a similar perspective. Figure 1 depicts the endocardial surfaces of the left and right ventricle, respectively, on which are marked the cable as well as sheet representations of the conduction system. Figure 2 shows horizontal and longitudinal sections of the ventricles depicting the nested ellipsoids of revolution used to approximate the myocardial walls. One set of confocal ellipsoids was used for the left ventricle and septum, and a second set for the right ventricular free wall. Fiber direction α corresponding to each individual ellipsoid was assumed constant, but varied from $+60^\circ$ to -60° from endocardium to epicardium. Thus, at midwall the cardiac fibers are circumferential with α

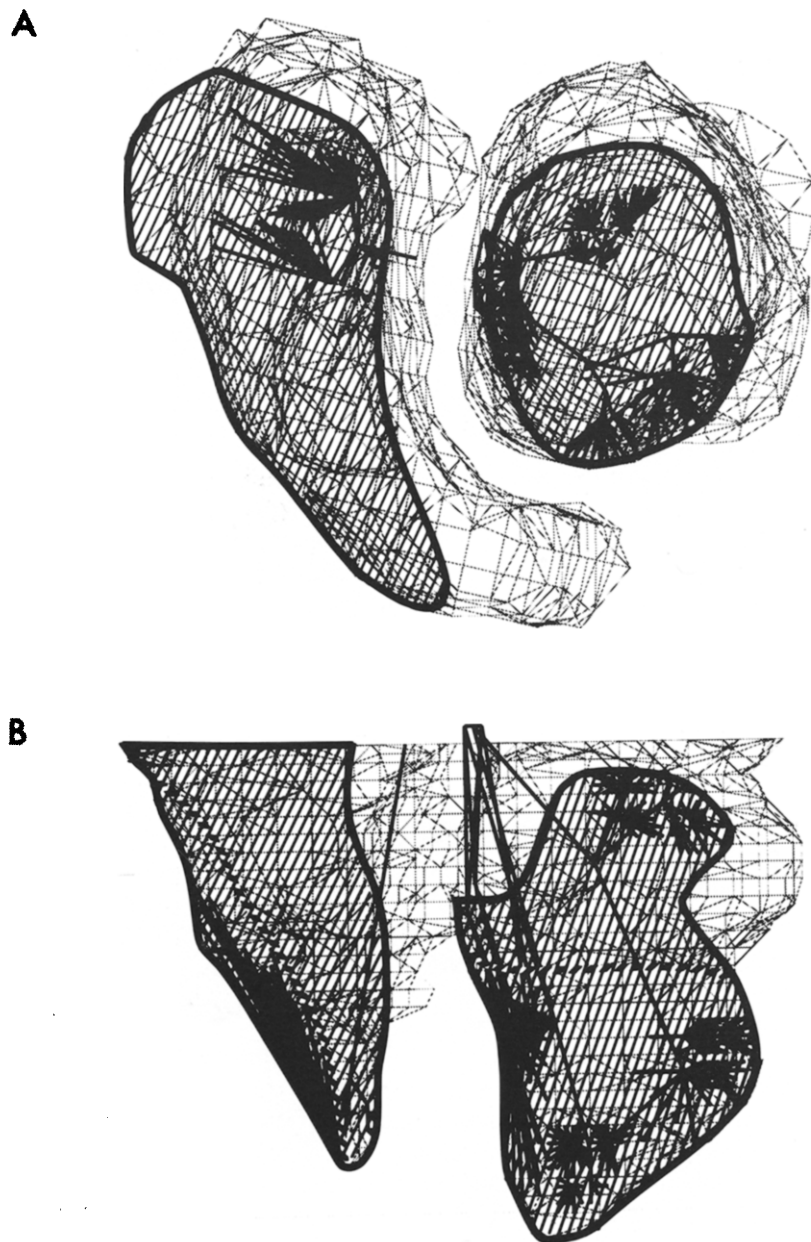


Fig. 1. Wire frame representations of the right and left ventricular endocardium are shown, as viewed from the top (A) and front (B), on which the cable and sheet representations of the conduction system are superposed.

being equal to zero. Moreover the variation in α with distance across the wall was represented by a cubic rather than a linear polynomial so as to better approximate the data of Streeter et al.^{3,4}

Isochrone Simulations

Figure 3 shows the atrial isochrones generated by the model following initiation of excitation in the three zones around the superior vena cava. A superior view of the heart is presented to enable better visualization of both atria. Plate 3 shows horizontal

and longitudinal sections of the heart depicting the intramural isochrones. Figure 4 depicts anterior, left lateral, and inferior views of the epicardium, on which the epicardial isochrones corresponding to normal activation have been plotted. The earliest epicardial breakthrough on the anterior right ventricle is clearly seen. These epicardial isochrones are qualitatively similar to those described by Wyndham et al.²⁸ for the *in situ* human heart. It must be stressed that the isochrones shown in Figure 4 are those that resulted following the iterative trial and error simulation process described in the Materials and Methods section, and that these isochrones give rise to the

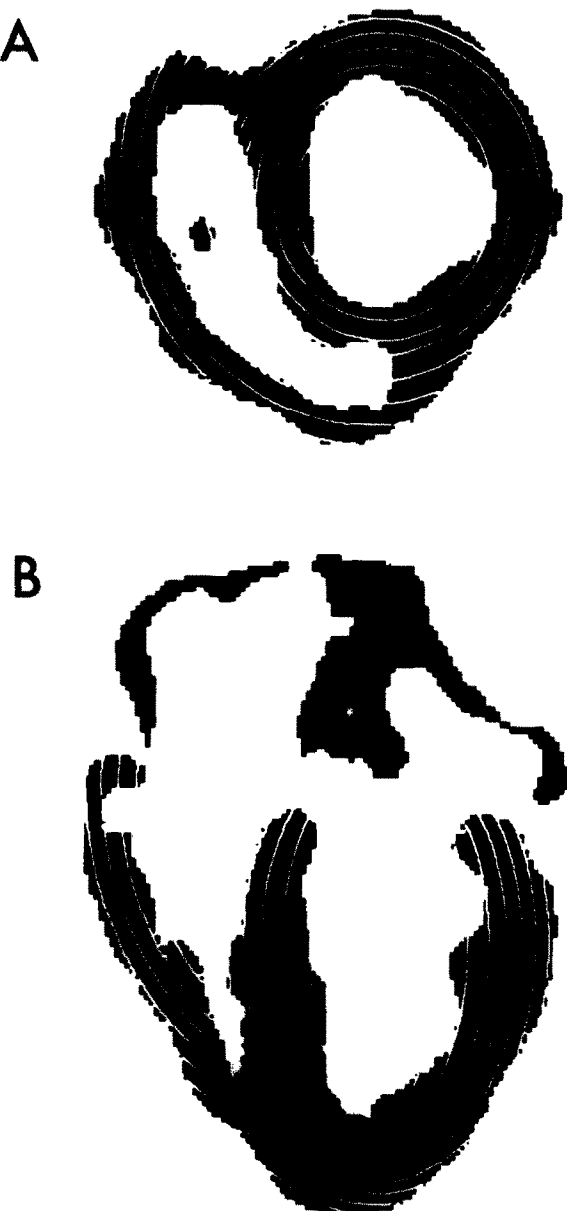


Fig. 2. Horizontal (A) and longitudinal (B) sections through the heart model are presented, depicting the ellipsoids of revolution used to approximate the ventricular myocardium. Fiber orientation (not shown) varies smoothly from one ellipsoid to the next.

normal ECG, VCG, and BSPM shown in the next subsection.

Surface Potential Simulations

Plate 4 shows anterior and left lateral views of the model heart as eventually positioned within the torso model. Figure 5A shows an apparently erratic Frank

VCG generated by the 25 atrial dipoles during the P wave. Since each atrial dipole contributes a small surface potential, the instant-by-instant variation in its contribution is relatively large. The VCG of Figure 5A has been calculated and plotted at 1-ms intervals with high-frequency components up to 500 Hz, and it is consequently sensitive to atrial dipole variations. Figure 5B shows the same VCG using a 9-point unity-gain moving-average filter corresponding to an extinction frequency of 111 Hz.²⁹ A much smoother P wave VCG results that compares favorably with the clinically observed normal P wave VCG.³⁰ Figure 6A shows the unfiltered ECG generated by all 88 regional dipoles of the heart model, and is within normal limits.¹² Figure 6B shows the unfiltered Frank VCG during QRS and T complexes and also appears normal.^{30,31} No filtering is needed with the QRS and T wave potentials owing to their larger amplitudes. Figure 7 depicts the BSPM at 18 instants during the cardiac cycle. These BSPMs are in agreement with those observed in normal subjects.³² Of particular interest is the local minimum on the anterior thorax at 201 ms, which is considered the surface manifestation of right ventricular breakthrough.

Discussion

The CT scan reconstruction technique is a very convenient way to obtain computer models of anatomic organs, since it automatically stacks serial sections one on top of the other with no rotational or translational misalignment. Not only is freezing in liquid nitrogen a rapid way to "fix" the anatomy, we also found that it led to a shrinkage of less than 1 mm in a prefreezing heart circumference of 232 mm. Tissue shrinkage is one reason why formaldehyde fixation is not used in heart model reconstruction. There also remains the problem of rigor mortis that prevents proper inflation of the ventricles and can only be overcome if the heart is obtained soon after death. Thus, in preliminary tests with freshly obtained canine hearts, we experienced much less difficulty in forcing open the ventricles.³³ Eventually, however, as the resolution of gated magnetic resonance imaging and CT scanners improve, these systems will be used for reconstructions of the *in vivo* beating heart. Indeed, recently, a canine heart model has been so reconstructed using magnetic resonance imaging.³⁴

Equation 1 describes the velocity of propagation for an arbitrary direction and assumes that each small segment of the activation wavefront can be represented as a plane wave. It represents a zero-order

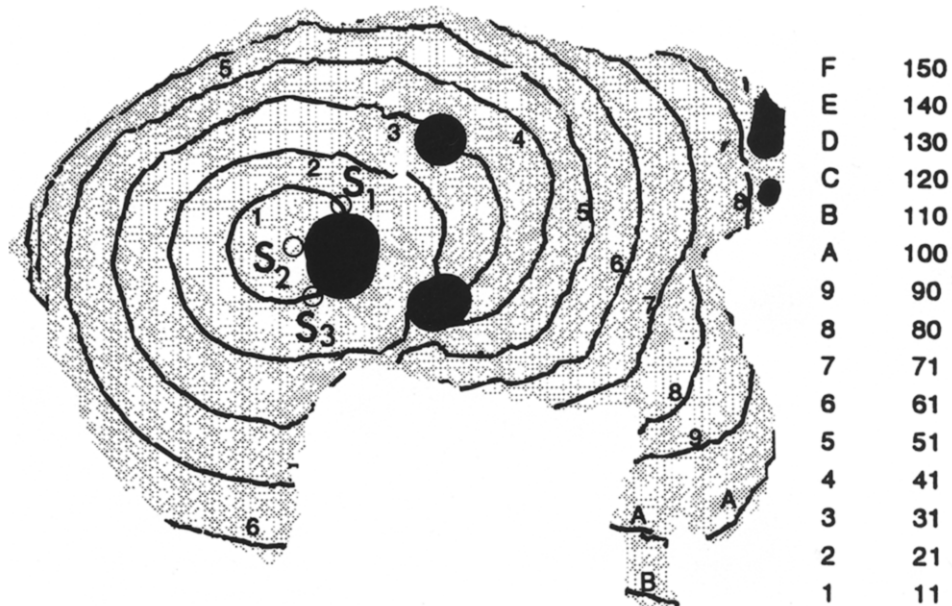
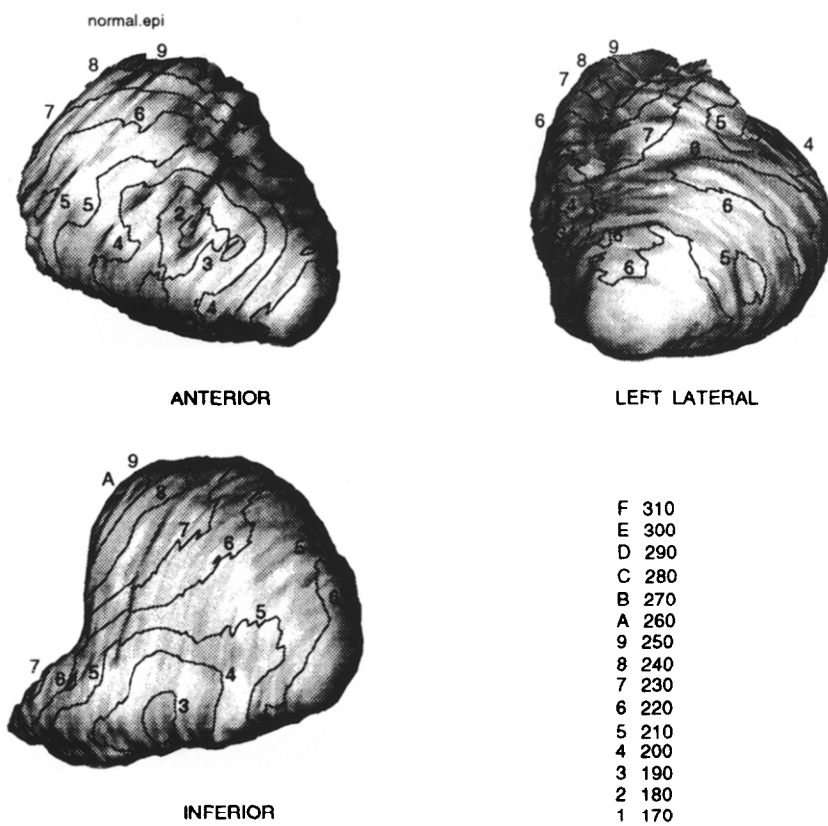


Fig. 3. Atrial isochrones generated by the model corresponding to normal excitation are shown on a superior view of the heart. The dark areas represent the sites of attachment of the atrial blood vessels. Points S_1 , S_2 , and S_3 represent the three pacemaker sites, with S_2 being excited 10 ms before S_1 and S_3 . The activation times corresponding to the isochrones are given alongside in the table.

Fig. 4. Anterior, left lateral, and inferior views of the heart, as positioned in the torso, are presented, on which the epicardial isochrones corresponding to normal activation have been plotted. The inferior view represents these isochrones as seen from the top through a supposedly transparent heart. The activation times (in ms following excitation of the pacemaker region S_2) corresponding to the isochrones are given in the table. Since left septal activation starts at 160 ms, the isochrones labeled 1, 2, . . . etc., respectively, represent the epicardial wavefront 10 ms, 20 ms, . . . etc. into ventricular activation.



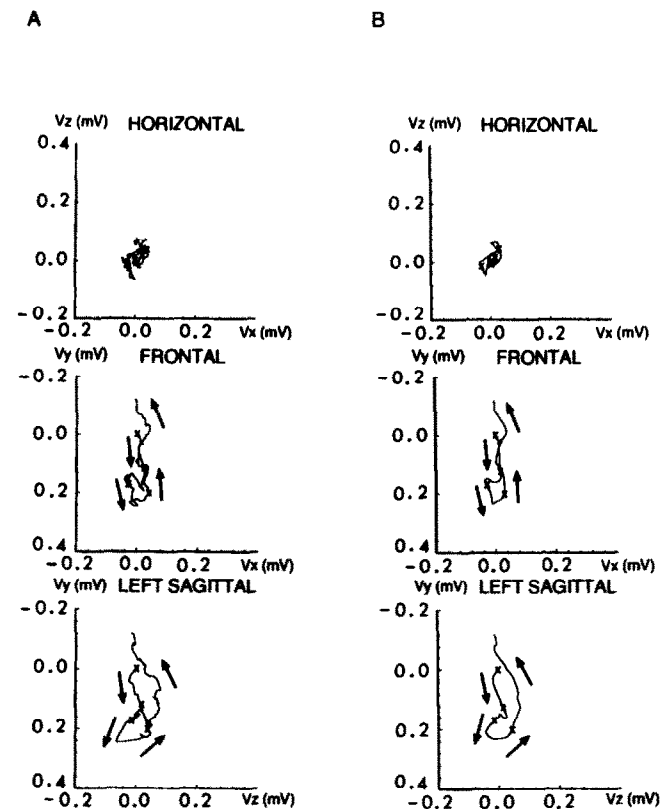


Fig. 5. (A) Simulated high-frequency Frank vectorcardiogram during the P wave. The four small crosses identify times 0, 20, 40, and 60 ms into the P wave, and serve to indicate the start of the P wave loops and hence the direction of the tracing. This direction is also indicated by the arrows alongside the loops. (B) Same vectorcardiogram, but this time following application of a nine-point moving average filter with an extinction frequency of 111 Hz.

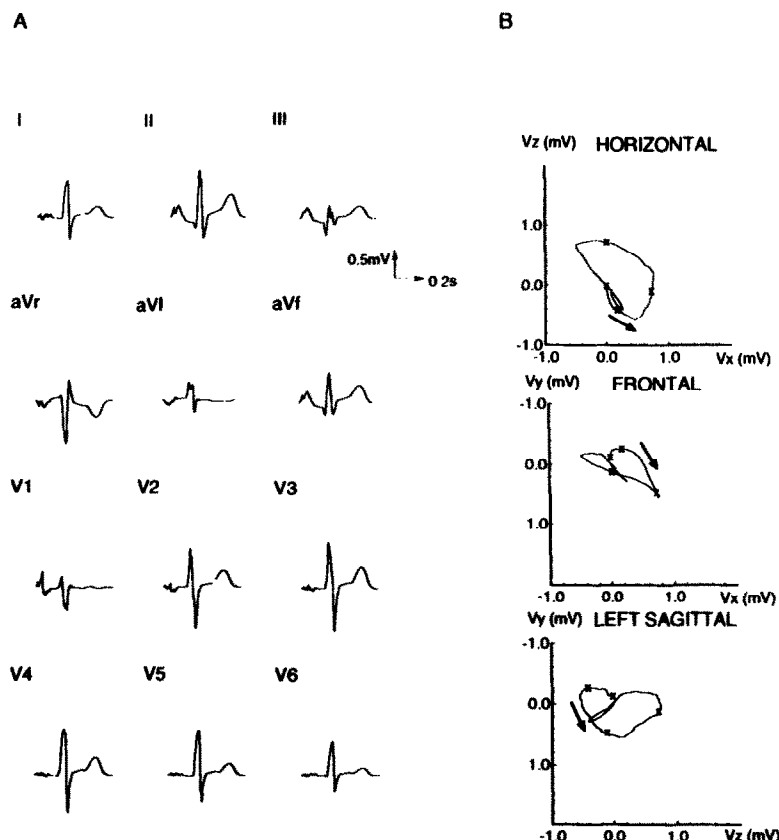


Fig. 6. (A) Normal unfiltered 12-lead ECG generated by the model. (B) Normal unfiltered Frank vectorcardiogram generated by the model. The four small crosses represent times 0, 20, 40, and 60 ms into the QRS, and serve to indicate the start of the QRS loops and hence the direction of the tracing. This direction is also indicated by the arrows beside the loops. The small T wave loops are also shown, but for clarity the P wave loops of Figure 5 have been suppressed.

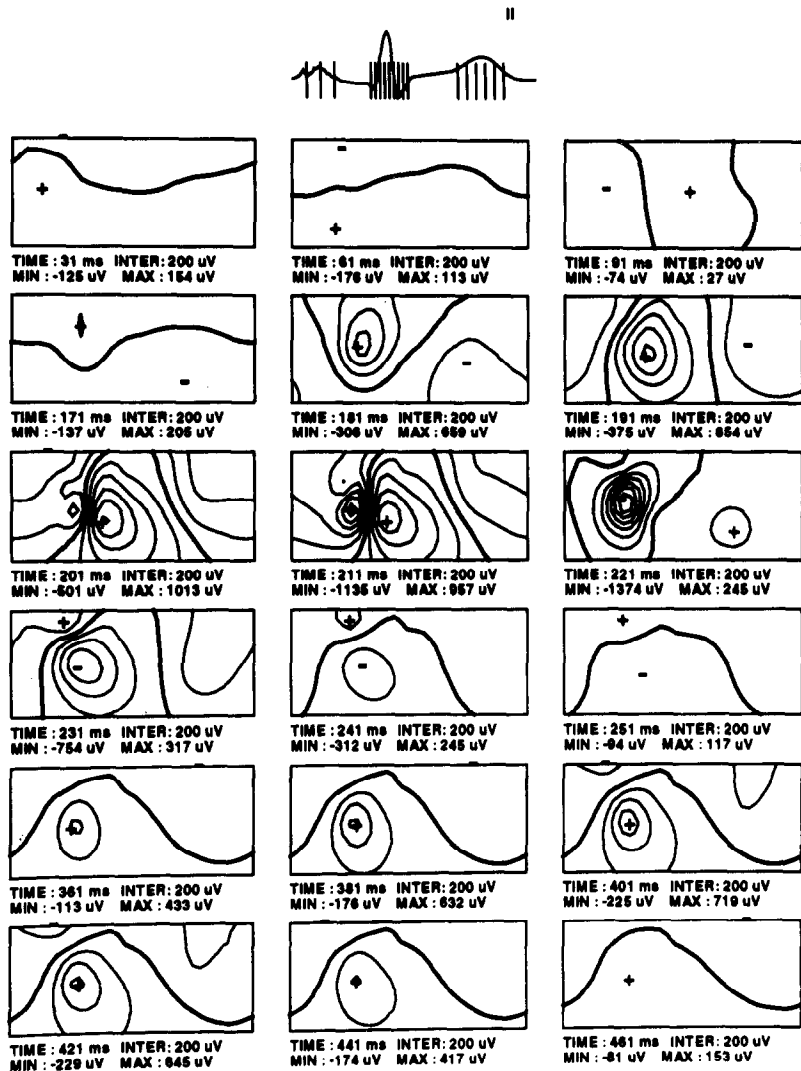


Fig. 7. Normal body surface potential maps simulated at 18 instants during the cardiac cycle (marked on the lead II ECG tracing shown). The left half of each body surface potential map represents the anterior chest and the right half the back. The zero isopotential is reinforced, and the location of the maximum and minimum are indicated by the plus and minus signs, respectively. Their values in microvolts are indicated below each map, as is the time into the cardiac cycle, measured after sinus node excitation. Contour interval is kept fixed throughout at 200 μ V.

"eikonal" equation for wavefront propagation.³⁵ It was derived in a slightly different form by Roberts et al.²¹ who showed that following point stimulation in an anisotropic bidomain characterized by a uniform fiber direction, it resulted in nearly ellipsoidal isochrones. It is thus equivalent to using an ellipsoidal Huygens principle construction for determining activation wavefronts and represents an extension of the spherical Huygens principle construction first employed in heart models by Solomon and Selvester.³⁶ The spherical Huygens principle entails the construction of spherical surfaces of radius $v\Delta t$ around every currently active model point, where v is the isotropic propagation velocity and Δt the desired isochrone interval. All nonactivated model points that fall within these spheres are considered activated at time $t + \Delta t$, and the envelope of these newly activated points determines the wavefront at $t + \Delta t$. The ellipsoidal Huygens construction simply replaces the spheres with ellipsoids of major and minor semiaxes

$v_l\Delta t$ and $v_t\Delta t$, respectively, where v_l and v_t are the velocities along and transverse to the local fiber direction. Needless to say, the ellipsoids are all oriented with their major axes along their respective local fiber directions. There is, however, an important advantage to using equation 1 rather than the ellipsoidal Huygens principle construction. With the Huygens construction the temporal resolution is limited by the choice of the time increment Δt , which must be sufficiently large so that the ellipsoids extend at least up to, if not beyond, the nearest neighbors along both major and minor axes. Furthermore, at each time step, because the surface of the isochrone-determining ellipsoids usually falls in between model points, a certain amount of truncation error results in only activating up to the enclosed point closest to the surface. Consequently, there is an overall loss in effective propagation velocity.³⁷ With equation 1 there is no limitation to the temporal resolution as the arrival times at nearest neighbors are calculated to 0.1 ms.

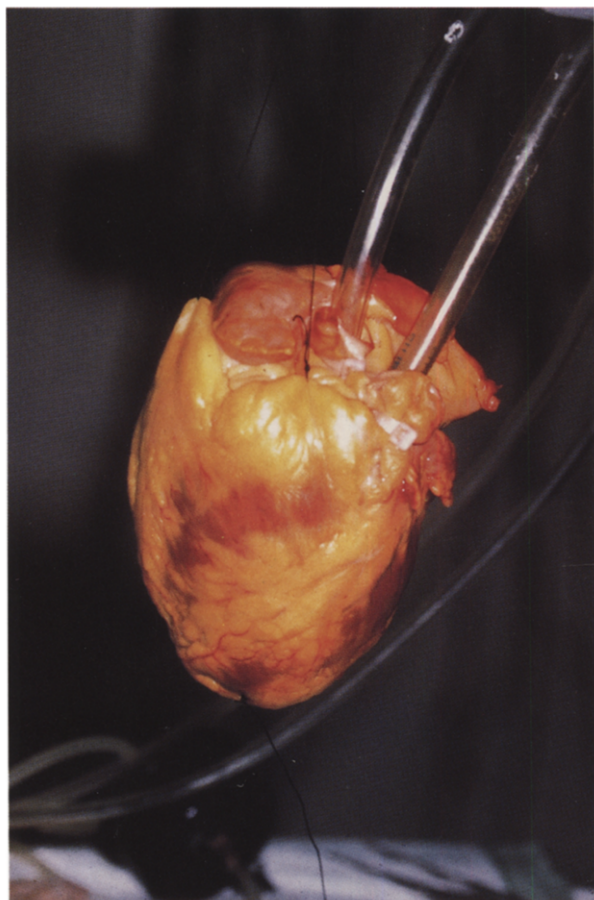


Plate 1

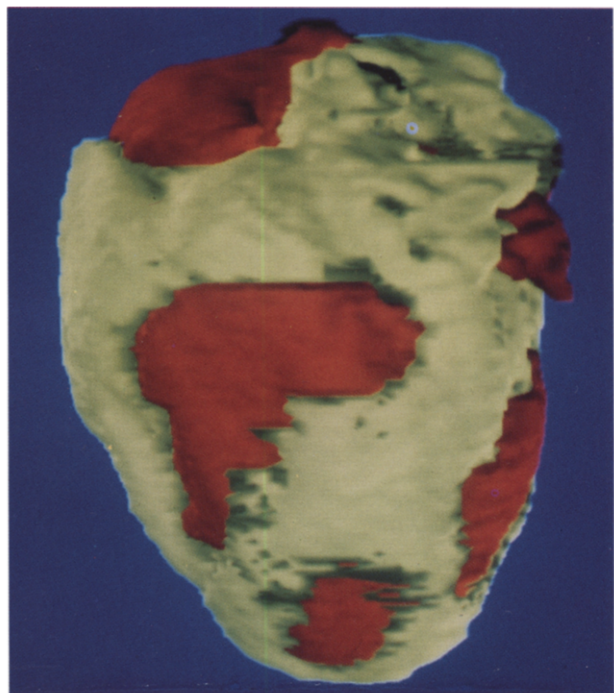


Plate 2

Plate 1. Anterior view of the cannulated and inflated human heart, photographed just prior to immersion in liquid nitrogen. The atrioventricular ring and left anterior descending coronary artery are covered by fatty issue.

Plate 2. Three-dimensional anterior view of the computer-generated model heart is shown. The brown regions represent active myocardium and the whitish regions the fat tissue seen in Plate 1.

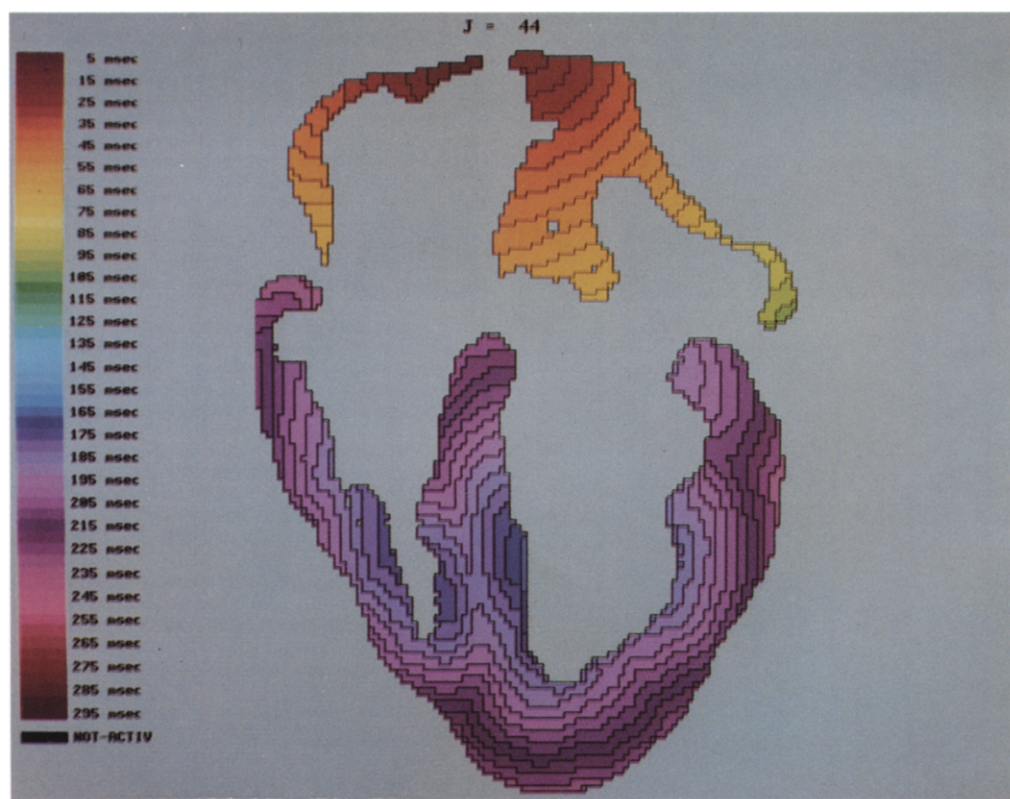
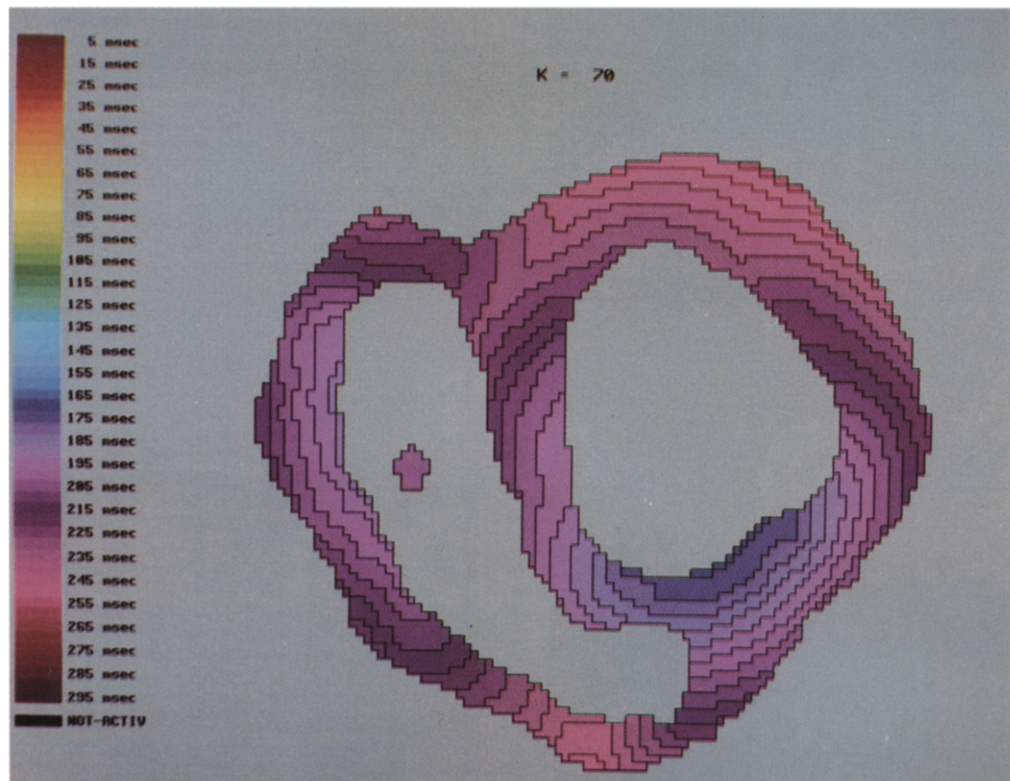


Plate 3

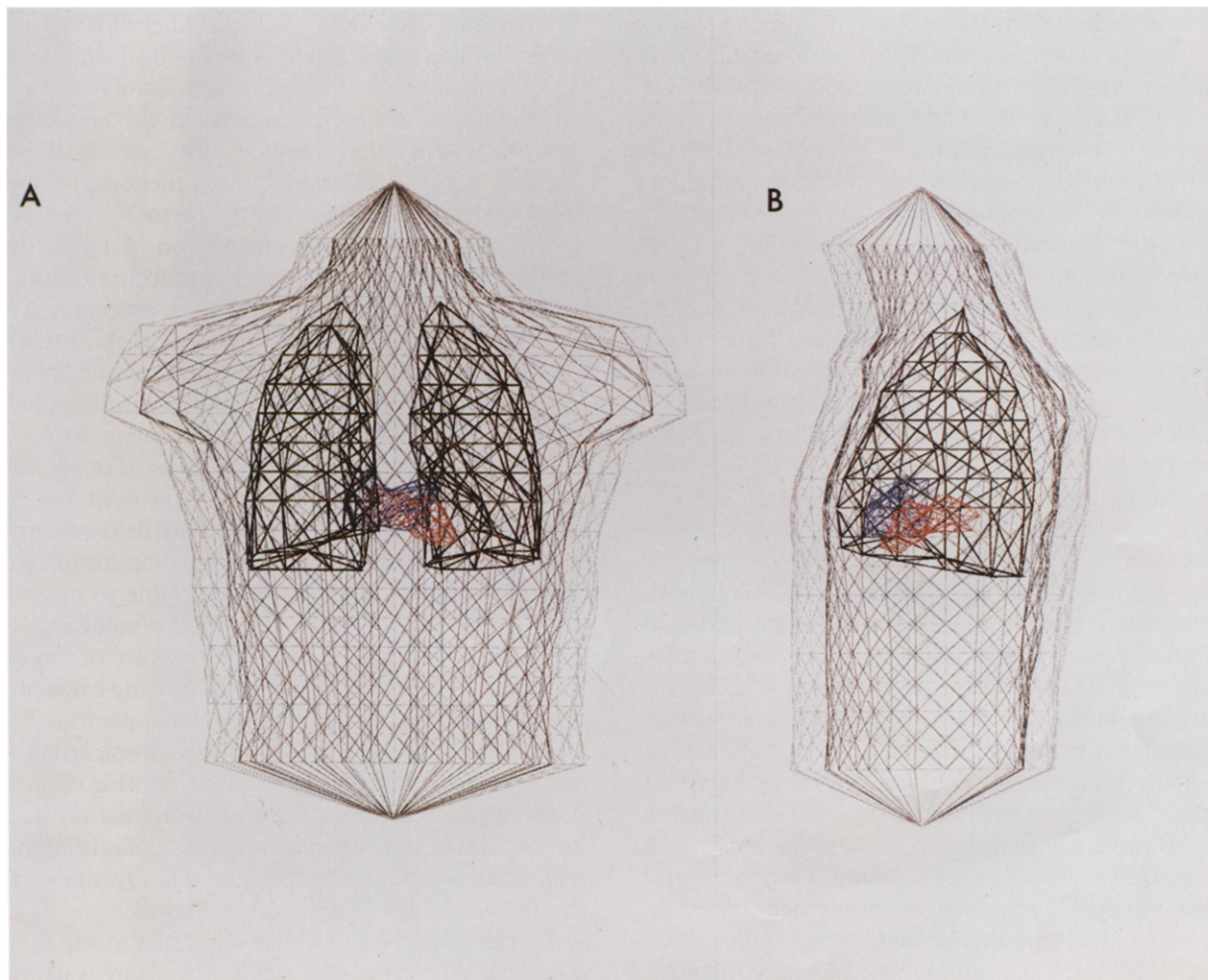


Plate 4

Plate 4. Anterior and left lateral views of the heart within the torso model. For clarity, only the right and left atrial and ventricular blood mass cavities are depicted, in blue and red, respectively. The epicardial surface of the model has been suppressed. While the lungs have been modeled and shown accurately, the skeletal muscle layer is only considered using the torso extension approach,²⁶ whereby the 1-cm thick anisotropic layer just beneath the surface is replaced by a 3-cm thick isotropic layer that extends the torso surface 2 cm outward. The isotropic layer, accordingly, exists between the two torso outlines, one representing the extended torso and the other the inner border of the muscle layer.

←
Plate 3. A horizontal section of the base of the ventricles (top) and a longitudinal section of atria and ventricles (bottom) illustrate the isochrones for normal activation of the heart model. The activation times corresponding to the colors are indicated on the left.

Furthermore, there is no rounding or truncation in these arrival times until the entire heart is activated, at which point each arrival time is rounded off to 1.0 ms. As a result, the propagation velocities used tend to be closer to measured values.

It has already been stated that equation 2 assumes an isotropic bidomain model for the myocardium. It results in equivalent dipole sources that are normal to the activation wavefront and are of uniform strength everywhere along it, existing in an isotropic interstitial monodomain. For an anisotropic bidomain myocardium that is homogeneous, two modifications arise. First, the equivalent dipole sources are oblique rather than normal to the wavefront due to an axial component of nonuniform strength that is aligned along the fiber direction and second, these dipole sources now exist in an anisotropic rather than an isotropic monodomain.^{2,19} With inhomogeneous anisotropy, that is, varying fiber direction in the myocardium, no exact equivalent dipole source formulation can be derived. Any use of oblique dipoles entails a concomitant assumption that the composite myocardium is homogeneous, and, to make the computations tractable, that it is also isotropic. Rather than make these assumptions we chose to continue to use equation 2. At this time we are unable to estimate the effects of ignoring myocardial anisotropy in surface potential computations. However, the similarity of our simulated potentials to measured ones, together with the fact that several earlier heart models² have also generated acceptable results using the isotropic approximation, may well mean that these effects are not overwhelming, especially with the simulation of normal activation when the wavefront moves across myocardial fibers. Under these conditions, the axial component of any equivalent oblique dipole source, being proportional to the component of the transmembrane potential gradient along the fibers, should become small.³⁸

A second area where the model may need some improvement is its spatial resolution. Although a 1-mm resolution would appear to be more than adequate, we found that altering the range of endocardial to epicardial fiber rotation from $\pm 60^\circ$ to $\pm 90^\circ$ led to very little change in the surface potentials. This was traced to the spatial resolution of 1 mm used in the model. Because of the cubic equation used to represent fiber rotation, most of the variation in fiber angle through the myocardial wall occurs over 2-mm thick layers at the endocardium and epicardium. The spatial resolution of the model is just not sufficient to alter propagation appreciably within the 2-mm endocardial layer (3 model points) and thereby manifest the increased fiber rotation. (Propagation differences were noted if fiber direction was disre-

garded completely and isotropic conduction assumed.) Furthermore, the use of the isotropic approximation for potential calculations eliminates the effect of increased fiber rotation on the equivalent dipole sources and hence on the surface potentials. Therefore, if the effects of altered fiber directions are to be simulated, the model may not be adequate. On the other hand, surface potential simulations with the model do reflect alterations in the conduction system parameters, such as velocity, geometry, and the site of Purkinje-myocardium junctions, or in the position of the heart within the torso.

We see that the spatial resolution of 1 mm used in the model is needed largely for accurate simulations of the propagation isochrones, especially if rotating fiber directions are included in the myocardium. For subsequent simulations of the far-field body surface potentials, acceptable results may be obtained by a much coarser arrangement of only 88 regional dipoles determined on the basis of equation 2. This may not hold if equation 2 is used as a first approximation to compute the near-field epicardial potentials. In this situation, rather than lumping dipoles by region, it might be preferable to compute these potentials from the elemental dipoles at every model point in some immediate vicinity of the epicardial point where the potential is being calculated. However, the assumption that the myocardium is isotropic is much more problematic with epicardial potential computations, and some accounting of the effects of fiber direction on dipole orientation needs to be considered. Indeed, accurate computation of epicardial potential distributions remains one of the challenges of the future.

Of the other heart models described in the literature that consider myocardial anisotropy, our own earlier lower-resolution (25,000 points vs 250,000) model³⁷ incorporated anisotropic propagation in an approximate manner by just reducing the conductivity in the endocardial to epicardial direction, with no accounting of the rotation of fiber direction in the plane perpendicular to this direction. The lower spatial resolution precluded the inclusion of any fiber rotation. Other computer models in which the fiber direction has been based on a detailed point-by-point histologic determination^{39,40} have been developed, but only used for the simulation of propagation without any concomitant surface potential computations. Still other models with a stylized fiber rotation similar to ours have been used for a study of the mechanics of ventricular contraction,^{41,42} for a simulation of propagation alone,⁴³ and for a simulation of propagation together with surface potential computations.⁴⁴⁻⁴⁷ Among these last models, the one by Killmann et al.⁴⁴ is similar to ours, but with fewer model

points (approximately 15,000) and also incorporated myocardial anisotropy only in the propagation algorithm and not in the calculation of the potentials. In the other, a model of a geometrically shaped simplified left ventricle alone, by Leon and Horacek,⁴⁵⁻⁴⁷ the fiber direction affected not only propagation but also the surface potentials. In other words, rather than use equation 2, the authors considered the equivalent dipole sources to be oblique to the wave-front. However, a precise accounting of the effect of myocardial anisotropy was not considered, since the oblique dipoles existed in a homogeneous isotropic myocardium. It is difficult to compare one heart model against another. Ultimately we feel that the best criterion is a model's performance in simulating the gamut of cardiac phenomena.

In this sense our model is reasonably versatile in that it can simulate a range of cardiac pathologies. Thus, in the companion paper⁵ we describe the simulation of the major conduction blocks. Ectopic beats and their associated BSPM patterns are also quite easy to simulate. Ischemia and infarction simulations may be realized, as described by Miller and Geselowitz,⁴⁸ by modifying the action potential of "ischemic" model points and by removing "infarcted" model points altogether. Reentrant arrhythmias can be obtained since each model point also has a predetermined absolute refractory period associated with it. This permits the reexcitation of any model point. Moreover, since the time of last activation of each point is stored in computer memory, it is also possible to make this absolute refractory period dependent on the previous cycle length as done by Killmann et al.⁴⁴ However, while the ECGs, VCGs, and BSPMs corresponding to these reentrant arrhythmias can be accurately simulated, insights into the mechanisms of these arrhythmias is not possible because each model point is not represented as an excitable membrane that is triggered due to electrotonic coupling from its neighbors. Such a propagation model for myocardium would represent the desired ideal, but due to computer limitations is usually only used for simulations in two- and three-dimensional cardiac tissue blocks.⁴⁹ A recent exception is a realistic model of the His-Purkinje conduction tree alone, developed by Pollard and Barr,^{50,51} in which electrotonic coupling and the Ebihara-Johnson membrane model⁵² is used to simulate propagation within the specialized conduction system. A more feasible approach for the whole heart is illustrated by Leon and Horacek's⁴⁵⁻⁴⁷ recently published model of the simplified left ventricle that represents each point with a simple sub-threshold resistance-capacitance network. When, due to electrotonic coupling, a threshold value is reached, a predefined action potential is elicited at

the point in question. This represents a compromise of intermediate complexity between the ideal simulation wherein electrotonic coupling and a full excitable membrane model for each point are used and our own approach where no coupling is used but an action potential is assumed triggered by plane wave propagation from a neighbor. Leon and Horacek's approach, when used with a realistic anatomy model, represents the next logical step in the evolution of computer heart models. This group has, in fact, already described some interesting preliminary results with such kinds of heart models.^{53,54}

Acknowledgments

The authors would like to express their appreciation and gratitude to Dr. Nicolas Mandalenakis for providing autopsy hearts, Pierre Fortier for his invaluable assistance with the preparation and freezing of the human heart, Sylvie Leclair and Suzanne Grisé for performing the CT scans, Jacques de Guise and Yves Martel for showing how to use the image segmentation and three-dimensional visualization routines written by them, and Abdelkader Mokrane, Hilda Hasswani, and Sébastien Lavier for help with the TECPLLOT software used to prepare some of the illustrations.

References

1. Plonsey R, Barr RC: Mathematical modeling of electrical activity of the heart. *J Electrocardiol* 20:219, 1987
2. Gulrajani RM: Models of the electrical activity of the heart and computer simulation of the electrocardiogram. *Crit Rev Biomed Eng* 16:1, 1988
3. Streeter DD Jr, Spotnitz HM, Patel DJ et al: Fiber orientation in the canine left ventricle during diastole and systole. *Circ Res* 24:339, 1969
4. Streeter DD Jr: Gross morphology and fiber geometry of the heart. p. 61. In Berne RM, Sperelakis N, Geigert SR (eds): *Handbook of physiology. Section 2: The cardiovascular system. Vol. 1: The heart*. American Physiological Society, Williams and Wilkins, Baltimore, 1979
5. Lorange M, Gulrajani RM, Nadeau RA, Prédé I: A computer heart model incorporating anisotropic propagation. II. Simulations of conduction block. *J Electrocardiol* 26:263, 1993
6. Eifler WJ, Macchi E, van Eck HJR et al: Mechanism of generation of body surface electrocardiographic P-waves in normal, middle, and lower sinus rhythms. *Circ Res* 48:168, 1981

7. de Guise J, Martel Y, Melillo M, Drouin G: Computerized three-dimensional reconstruction of biological structures for biomedical modeling. p. 59. In Proc 1987 IEEE Montech Conf, 1988
8. de Guise JA, Martel Y: 3D-biomedical modeling: merging image processing and computer aided design. p. 426. In Proc Ann Int Conf IEEE Eng Med Biol Soc, 1988
9. Lorange M, Gulrajani RM, de Guise J, Fortier P: A whole-heart model incorporating myocardial anisotropy. p. 195. In Proc Ann Conf IEEE Eng Med Biol Soc, 1988
10. Lorange M: Simulation des blocs de conduction à l'aide d'un modèle de cœur humain incorporant la propagation anisotropique. PhD thesis. Ecole Polytechnique, Montréal, 1991
11. Boineau JP, Schuessler RB, Mooney CR et al: Multicentric origin of the atrial depolarization wave: the pacemaker complex. Relation to dynamics of atrial conduction, P-wave changes and heart rate control. Circulation 58:1036, 1978
12. Cooksey JD, Dunn M, Massie E: Clinical vectorcardiography and electrocardiography. Year Book Medical, Chicago, 1977
13. Boineau JP, Schuessler RB, Hackel DB et al: Multicentric distribution and rate differentiation of the atrial pacemaker system: pacemaker complex. p. 221. In Little RC (ed): Physiology of atrial pacemakers and conductive tissues. Futura Publishing, Mount Kisco, NY, 1980
14. Lazzara R, Yeh BK, Samet P: Functional anatomy of the canine left bundle branch. Am J Cardiol 33:623, 1974
15. Nagao K, Toyama J, Kodama I, Yamada K: Role of the conduction system in the endocardial spread in the right ventricle. Am J Cardiol 48:864, 1981
16. Myerburg RJ, Nilsson K, Gelband H: Physiology of canine intraventricular conduction and endocardial excitation. Circ Res 30:217, 1972
17. Veenstra RD, Joyner RW, Rawling DA: Purkinje and ventricular activation sequences of canine papillary muscle: effects of quinidine and calcium on the Purkinje-ventricular conduction delay. Circ Res 54:500, 1984
18. Durrer D, van Dam RTh, Freud GE et al: Total excitation of the isolated human heart. Circulation 41:899, 1970
19. Colli-Franzone P, Guerri L, Viganotti C: Oblique dipole layer potentials applied to electrocardiology. J Math Biol 17:93, 1983
20. Plonsey R, Barr RC: Current flow patterns in two-dimensional anisotropic bisyncytia with normal and extreme conductivities. Biophys J 45:557, 1984
21. Roberts DE, Hersh LT, Scher AM: Influence of cardiac fiber orientation on wavefront voltage, conduction velocity, and tissue resistivity in the dog. Circ Res 44: 701, 1979.
22. Roberts DE, Scher AM: Effect of tissue anisotropy on extracellular potential fields in canine myocardium in situ. Circ Res 50:342, 1982
23. Katz AM: Physiology of the heart. Raven Press, New York, 1977
24. Burgess MJ, Green LS, Millar K et al: Sequence of normal ventricular recovery. Am Heart J 84:660, 1972
25. Sekiya S, Ichikawa S, Tsutsumi T, Harumi K: Distribution of action potential durations in the canine left ventricle. Jpn Heart J 25:181, 1984
26. McFee R, Rush S: Qualitative effects of thoracic resistivity variations on the interpretation of electrocardiograms: the low resistance surface layer. Am Heart J 76:48, 1968
27. Gulrajani RM, Mailloux GE: A simulation study of the effects of torso inhomogeneities on electrocardiographic potentials, using realistic heart and torso models. Circ Res 52:45, 1983
28. Wyndham CR, Meeran MK, Smith T et al: Epicardial activation of the intact human heart without conduction defect. Circulation 59:161, 1979
29. Oppenheim AV, Willsky AS, Young IT: Signals and systems. Prentice-Hall, Englewood Cliffs, NJ, 1983
30. Chou T-C, Helm RA, Kaplan S: Clinical vectorcardiography. Grune and Stratton, New York, 1974
31. Reddy CVR, Gould LA: Correlative atlas of vectorcardiograms and electrocardiograms. Futura Publishing, Mount Kisco, NY, 1977
32. Taccardi B, de Ambroggi L, Viganotti C: Body-surface mapping of heart potentials. p. 436. In Nelson CV, Geselowitz DB (eds): The theoretical basis of electrocardiology. Clarendon Press, Oxford, 1976
33. Lorange M, de Guise J, Gulrajani RM, Fortier P: Computerized construction of a heart model using a CT scan. p. 97. In Proc 14th Can Med Biol Eng Soc Conf, 1988
34. Cresswell LL, Wyers SG, Pirolo JS et al: Mathematical modeling of the heart using magnetic resonance imaging. IEEE Trans Med Imaging 11:581, 1992
35. Colli-Franzone P, Guerri L, Tentoni S: Mathematical modeling of the excitation process in myocardial tissue: Influence of fiber rotation on wavefront propagation and potential field. Math Biosci 101:155, 1990
36. Solomon JC, Selvester RH: Simulation of measured activation sequence in the human heart. Am Heart J 85:518, 1973
37. Lorange M, Gulrajani RM: Computer simulation of the Wolff-Parkinson-White preexcitation syndrome with a modified Miller-Geselowitz heart model. IEEE Trans Biomed Eng, 33:862, 1986
38. Colli-Franzone P, Guerri L, Viganotti C et al: Potential fields generated by oblique dipole layers modeling excitation wavefronts in the anisotropic myocardium: comparison with potential fields elicited by paced dog hearts in a volume conductor. Circ Res 51:330, 1982
39. Saxberg BEH, Grumbach MP, Cohen RJ: A time dependent anatomically detailed model of cardiac conduction. p. 401 In Ripley KL (ed): Computers in cardiology. IEEE Computer Society Press, Washington, 1985
40. Hunter PJ, Small BH: The analysis of cardiac function: a continuum approach. Prog Biophys Mol Biol 52: 101, 1988

41. Beyar R, Sideman S: A computer study of the left ventricular performance based on fiber structure, sarcomere dynamics, and transmural electrical propagation velocity. *Circ Res* 55:358, 1984
42. Sideman S, Beyar R, Azhari H et al: Three-dimensional computer simulation of the cardiac system. *Proc IEEE* 76:708, 1988
43. Adam D: Propagation of depolarization and repolarization processes in the myocardium: an anisotropic model. *IEEE Trans Biomed Eng* 38:133, 1991
44. Killmann R, Wach P, Dienstl F: Three-dimensional computer model of the entire human heart for simulation of reentry and tachycardia: gap phenomenon and Wolff-Parkinson-White syndrome. *Basic Res Cardiol* 86:485, 1991
45. Leon LJ, Horacek BM: Computer model of excitation and recovery in the anisotropic myocardium. I. Rectangular and cubic arrays of excitable elements. *J Electrocardiol* 24:1, 1991
46. Leon LJ, Horacek BM: Computer model of excitation and recovery in the anisotropic myocardium. II. Excitation in the simplified left ventricle. *J Electrocardiol* 24:17, 1991
47. Leon LJ, Horacek BM: Computer model of excitation and recovery in the anisotropic myocardium. III. Arrhythmogenic conditions in the simplified left ventricle. *J Electrocardiol* 24:33, 1991
48. Miller WT, Geselowitz DB: Simulation studies of the electrocardiogram. II. Ischemia and infarction. *Circ Res* 43:315, 1978
49. Pollard AE, Hooke N, Henriquez CS: Cardiac propagation simulation. p. 319. In Pilkington TC, Loftis B, Thompson JF et al (eds): *High performance computing in biomedical research*. CRC Press, Boca Raton, FL, 1993
50. Pollard AE, Barr RC: The construction of an anatomically based model of the human ventricular conduction system. *IEEE Trans Biomed Eng* 37:1173, 1990
51. Pollard AE, Barr RC: Computer simulations of activation in an anatomically based model of the human ventricular conduction system. *IEEE Trans Biomed Eng* 38:982, 1991
52. Ebihara LH, Johnson EA: Fast sodium current in cardiac muscle: a quantitative description. *Biophys J* 32: 779, 1980
53. Nenonen J, Edens JA, Leon LJ, Horacek BM: Computer model of propagated excitation in the anisotropic human heart. I. Implementation and algorithms. p. 545. In Ripley K, Murray A (eds): *Proceedings of the 1991 Computers in Cardiology Conference*. IEEE Computer Society Press, Los Alamitos, CA, 1992
54. Nenonen J, Edens JA, Leon LJ, Horacek BM: Computer model of propagated excitation in the anisotropic human heart: II. Simulation of extracardiac fields. p. 217. In Ripley K, Murray A (eds): *Proceedings of the 1991 Computers in Cardiology Conference*. IEEE Computer Society Press, Los Alamitos, CA, 1992